APPLIED PHYSICS LETTERS **99**, 063509 (2011)

Numerical investigation into the switchable diode effect in metal-ferroelectric-metal structures

Chen Ge, Kui-Juan Jin,[a)] Can Wang, Hui-Bin Lu, Cong Wang, and Guo-Zhen Yang
Beijing National Laboratory for Condensed Matter Physics, Institute of Physics, Chinese Academy of Sciences, Beijing 100190, China

(Received 17 May 2011; accepted 24 July 2011; published online 10 August 2011)

A self-consistent numerical model, particularly including the incomplete screening effect of metal electrodes, is introduced to reveal the mechanism of the switchable diode characteristics in metal/ferroelectric/metal structures. The calculated results are in good agreement with recent experimental data, theoretically demonstrating the important role played by the polarization-modulated barrier. Our calculations confirm that electrodes with a smaller permittivity, such as noble metals, are better choices to obtain a more pronounced switchable diode effect, and the barrier height variation as a function of the polarization will deviate from the linear relationship if the carrier concentration induced by the polarization becomes sufficiently high. © *2011 American Institute of Physics*. [doi:10.1063/1.3624849]

Recently, much attention has been paid to the switchable diode effect induced by pulse voltages in metal/ferroelectric/metal (MFM) structures, due to its potential application in non-volatile memories.[1–4] In this paper, we propose a self-consistent model, particularly including the incomplete screening effect of realistic metal electrodes,[5] to describe the switchable diode effect in MFM structures, and the model will be applied to our recent experimental phenomenon measured in the $SrRuO_3$(SRO)/$BiFeO_3$(BFO)/Pt structure.[2,3] Some important factors affecting the switchable diode characteristics in the structure are revealed theoretically.

In this one-dimensional model, we consider electron transport in the MFM structure as shown in Fig. 1, where NP, RP, and LP denote the states of non-polarization, right polarization, and left polarization, respectively. The ferroelectric is treated as a single domain structure. The fundamental equations are as follows:

$$\frac{d^2\phi(x)}{dx^2} = -\frac{e}{\varepsilon(x)}\rho(x), \tag{1}$$

$$\frac{1}{e}\frac{dj(x)}{dx} - R(x) = 0, \tag{2}$$

$$j(x) = \frac{\sigma(x)}{e}\frac{d\kappa(x)}{dx}, \tag{3}$$

where x is the spatial coordinate and e denotes the elementary charge. $\phi(x)$, $\varepsilon(x)$, $\rho(x)$, $j(x)$, $R(x)$, $\sigma(x)$, and $\kappa(x)$ represent the electrostatic potential, dielectric constant, charge density, current density, recombination rate, conductivity, and electrochemical potential, respectively. Here, we only consider the electron transport for n-type BFO and electrodes, and the recombination rate is taken as zero.

For metals, the conductivity is given by $\sigma_m(x) = e\mu_m n_m(x)$, where μ_m and $n_m(x)$ denote the mobility and electron density, respectively. We employ the well-known free electron model and the Thomas-Fermi approximation.[6] Then, the electrochemical potential of the metal $\kappa_m(x)$ is given by[7]

$$\kappa_m(x) = \frac{\hbar^2}{2m}[3\pi^2 n_m(x)]^{\frac{2}{3}} - e\phi(x), \tag{4}$$

where $\hbar$ is the reduced Planck constant and m denotes the effective electron mass.

For ferroelectric semiconductors, the conductivity $\sigma_s(x)$ is written as $\sigma_s(x) = e\mu_s n_s(x)$. The electrochemical potential $\kappa_s(x)$ reads

$$\kappa_s(x) = kT\ln\left[\frac{n_s(x)}{Nc}\right] + E_c - e\phi(x), \tag{5}$$

where k, T, and E_c are the Boltzmann constant, the temperature, and the bottom of conduction band, respectively. The effective density of states Nc is expressed as $Nc = 2(m_s kT/2\pi\hbar^2)^{3/2}$. Here m_s represents the electron effective mass of ferroelectric.

In our model, a simple approach is adopted, in which the ferroelectric polarization is regarded as an infinite thin sheet of charges located at the interfaces. Thus, the electrostatic properties at the interface can be characterized by the interface charge density σ, induced by the ferroelectric polarization P.[8]

$$\varepsilon_s\varepsilon_0\frac{d\phi(x)}{dx}\Big|_{X_l^+} - \varepsilon_m\varepsilon_0\frac{d\phi(x)}{dx}\Big|_{X_l^-} = -\sigma(X_l) = P, \tag{6}$$

$$\varepsilon_m\varepsilon_0\frac{d\phi(x)}{dx}\Big|_{X_r^+} - \varepsilon_s\varepsilon_0\frac{d\phi(x)}{dx}\Big|_{X_r^-} = -\sigma(X_r) = -P, \tag{7}$$

where X_l and X_r denote the positions of left and right interface, respectively. A simple boundary condition is employed to solve the continuity equation[7]

[a)]Author to whom correspondence should be addressed. Electronic mail: kjjin@iphy.ac.cn.

Author complimentary copy. Redistribution subject to AIP license or copyright, see http://apl.aip.org/apl/copyright.jsp

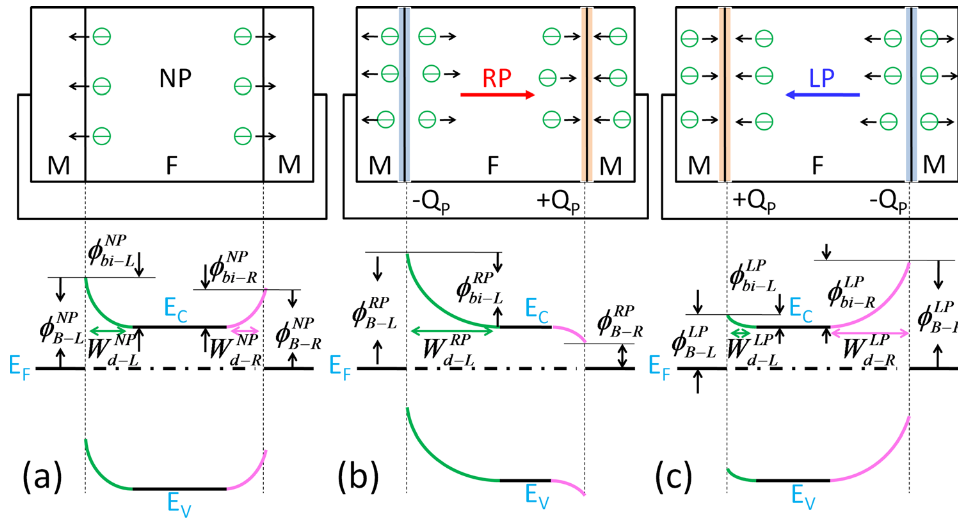

FIG. 1. (Color online) The schematic structures and band diagrams of the MFM device under short circuit conditions in the case of non-polarization (NP) (a), right polarization (RP) (b), and left polarization (LP) (c). The arrow denotes the direction of the polarization. Q_P is the polarization charge; ϕ_{B-L} (ϕ_{B-R}) is the barrier height; ϕ_{bi-L} (ϕ_{bi-R}) is the built-in potential; W_{d-L} (W_{d-R}) is the width of depletion region. Here L and R used as subscripts represent the left and right interface, respectively.

$$\kappa(x) = continuous. \tag{8}$$

Then, these equations can be self-consistently solved using the iterative method.

It is necessary to clarify the effect of the metal-ferroelectric interface on the band diagrams, the charge density distributions, and the transport behaviors in MFM structures. Here, we consider two model systems, two ferroelectric materials, F1 and F2, with the same metal material M as two electrodes, respectively, M/F1/M and M/F2/M. The difference between F1 and F2 is that the electron affinity and work function of F1 are (0.4 eV) larger than those of F2, respectively. The length of the whole system is set as 300 nm, and the thickness of the metal is chosen as 30 nm. The ferroelectric polarization is assumed to be $P = \pm 30\,\mu C/cm^2$. In this paper, the positive and negative polarization values are defined to be RP and LP, respectively. The parameters for calculations are listed in Table I. From Figs. 2(a) and 2(b), ϕ_{B-L}, ϕ_{bi-L} and W_{d-L} increase while ϕ_{B-R}, ϕ_{bi-R}, and W_{d-R} decrease in the case of RP compared to the case of NP. On the contrary, ϕ_{B-L}, ϕ_{bi-L}, and W_{d-L} decrease while ϕ_{B-R}, ϕ_{bi-R} and W_{d-R} increase in the case of LP compared to the case of NP. Electrons in part of F1 are depleted whereas electrons in the whole F2 are depleted. Therefore, M/F1/M behaves as a diode, and the conduction direction of the diode could be reversed by polarization reversal. The corresponding *J-V* curves are shown in Figs. 2(c1) and 2(c2). For M/F2/M, similar transport behaviors could be observed as exhibited in Figs. 2(c3) and 2(c4). In brief, the polarization could modulate the barrier at the interfaces, which plays a dominant role in the mechanism of the switchable diode characteristics in MFM structures.

This model is applied to our recent experimental data of SRO/BFO/Pt.[2,3] *I-V* curves with a sweep voltage of ±2 V, as shown in Fig. 3, were measured, indicating no evident hysteretic behavior. More details about the experiment can be found in Ref. 3. In our calculations, we regard SRO and Pt as the left and right electrodes, respectively. The length of the BFO film is 240 nm, and the thickness of the metals is set as 30 nm. For our BFO, the saturation polarization value is about 65 μC/cm^2.[3] The band-gap of BFO is about 2.6 eV.[9] The BFO film can be regarded as an *n*-type semiconductor owing to the naturally produced oxygen vacancies. Here, the work functions of SRO, BFO, and Pt are chosen as 5.0 eV (reported 4.8-5.2 eV),[10–12] 4.7 eV (Ref. 13), and 5.55 eV (reported 5.3-5.7 eV),[12,14] respectively. The electron effective masses of SRO, BFO, and Pt are 5m$_0$ (reported 3.7-7),[15,16] 5m$_0$,[17] and m$_0$, respectively. The relative dielectric constant of SRO is approximately 8.[16] The dielectric constant of Pt is chosen as 2 (typically, $\varepsilon = 2-4$ for noble metals). The measured dielectric constant of as-grown BFO is about 50.[3] However, the dielectric constant of pure BFO without electrodes would be larger than that of SRO/BFO/Pt due to a finite screening length in metals.[5] Therefore, the dielectric constant is assumed to be 100 here. The parameters for calculations are listed in Table I. The good agreement between the theoretical results and experimental data, as shown in Fig. 3, reveals that the model can be used to analyze the transport property in MFM structures.

In order to further understand the switchable diode phenomenon, we calculate the barrier height variation, defined as $\Delta\phi = \phi_B^P - \phi_B^{NP}$, as a function of the polarization in the SRO/BFO/Pt structure. The calculated dependence of $\Delta\phi$ on the polarization is exhibited in Fig. 4, which mostly shows the linear relationship. From Fig. 4, $|\Delta\phi_{Pt/BFO}|$ is larger than $|\Delta\phi_{SRO/BFO}|$ under the same polarization, mainly owing to the smaller permittivity of Pt. Therefore, electrodes with a smaller permittivity, such as noble metals, are better choices to obtain a more pronounced switchable diode effect. Moreover, $\Delta\phi_{Pt/BFO}$ as a function of the polarization shows a deviation away from the linear dependence in the case of large RP. Under a polarization large enough the electron concentration could be rather high (2.0×10^{20} cm^{-3} under a polarization of 150 μC/cm^2). Thus, the screening effect of the ferroelectric is significant compared with that of the

TABLE I. The parameters used in our calculations.

	SRO	Pt (M)	BFO	F1 (F2)
Dielectric constant (ε_0)	8	2	100	100
Mobility (cm^2/(V·s))	10	60	5	5
Effective mass (m$_0$)	5	1	5	5
Concentration (cm^{-3})	1.2×10^{22}	1.5×10^{22}	4×10^{16}	3×10^{17}
Work function (eV)	5.0	5.55	4.7	5.43 (5.03)

Author complimentary copy. Redistribution subject to AIP license or copyright, see http://apl.aip.org/apl/copyright.jsp

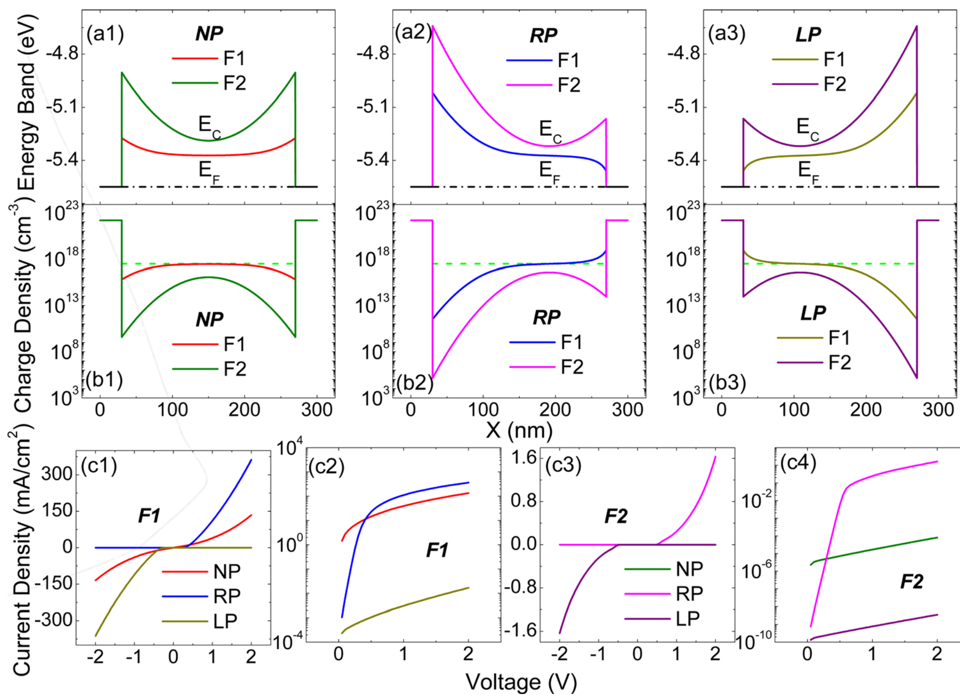

FIG. 2. (Color online) Band diagrams of M/F1/M and M/F2/M structures in the case of NP (a1), RP (a2), and LP (a3). Charge density distributions of M/F1/M and M/F2/M structures in the case of NP (b1), RP (b2), and LP (b3). The green dash line denotes the doping density 3×10^{17} cm^{-3} of F1 and F2. *J-V* curves of M/F1/M in the linear scale (c1) and the semi-logarithmic scale (c2), M/F2/M in the linear scale (c3), and the semi-logarithmic scale (c4).

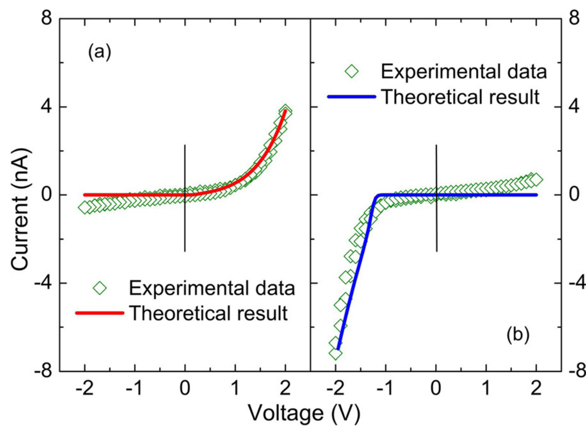

FIG. 3. (Color online) The experimental (diamonds) and calculated (lines) *I-V* in the case of RP (a) and LP (b) for the SRO/BFO/Pt structure.

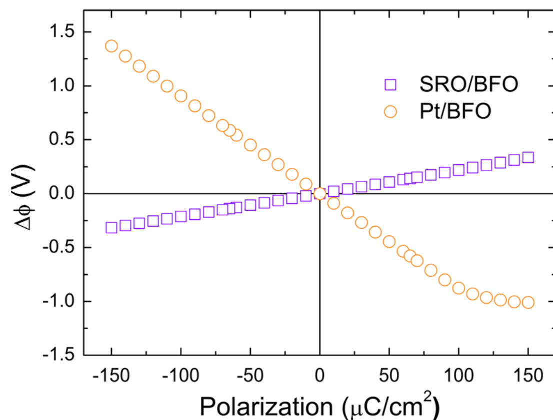

FIG. 4. (Color online) The calculated $\Delta\phi$ versus the polarization in the SRO/BFO/Pt structure.

metal, which gives rise to the deviation. Nevertheless, $\Delta\phi_{SRO/BFO}$ does not manifest this deviation in the case of large LP, because $\Delta\phi_{SRO/BFO}$ is smaller than $\Delta\phi_{Pt/BFO}$ under the same polarization and the electron concentration is only 2.1×10^{17} cm^{-3} under a polarization of -150 μC/cm^2.

In conclusion, based on the self-consistent calculation, it has been proved that the polarization-modulated barrier plays a dominant role in the mechanism of the switchable diode characteristics in MFM structures. It is hoped that the model would be helpful in promoting the further experimental development of the switchable diode effect in MFM structures.

This work has been supported by the National Natural Science Foundation of China and the National Basic Research Program of China.

[1]T. Choi *et al.*, Science **324**, 63 (2009).
[2]A. Q. Jiang *et al.*, Adv. Mater. **23**, 1277 (2011).
[3]C. Wang *et al.*, Appl. Phys. Lett. **98**, 192901 (2011).
[4]C. J. Won *et al.*, J. Appl. Phys. **109**, 084108 (2011).
[5]B. B. Mehta *et al.*, J. Appl. Phys. **44**, 3379 (1973); C. T. Black and J. J. Welser, IEEE Trans. Electron Devices **46**, 776 (1999).
[6]N. W. Ashcroft and N. D. Mermin, *Solid State Physics* (Thomson Learning, Florence, 1976).
[7]F. Neumann *et al.*, J. Appl. Phys. **100**, 084511 (2006); F. Neumann *et al.*, Phys. Rev. B **75**, 205322 (2007).
[8]D. Schröder, *Modelling of Interface Carrier Transport for Device Simulation* (Springer, Berlin, 1994).
[9]S. R. Basu *et al.*, Appl. Phys. Lett. **92**, 091905 (2008).
[10]M. van Zalk *et al.*, Phys. Rev. B **82**, 134513 (2010).
[11]M. Minohara *et al.*, Appl. Phys. Lett. **90**, 132123 (2007).
[12]R. Plonka *et al.*, Appl. Phys. Lett. **86**, 202908 (2005).
[13]H. Yang *et al.*, Appl. Phys. Lett. **92**, 102113 (2008).
[14]A. Javey *et al.*, Nature **424**, 654 (2003).
[15]G. Herranz *et al.*, Phys. Rev. B **77**, 165114 (2008).
[16]D. J. Kim *et al.*, Phys. Rev. Lett. **95**, 237602 (2005).
[17]C. H. Yang *et al.*, Nat. Mater. **8**, 485 (2009).

Author complimentary copy. Redistribution subject to AIP license or copyright, see http://apl.aip.org/apl/copyright.jsp